Anticancer Effects of Niclosamide in Human Glioblastoma

Anja Wieland, Daniel Trageser, Sabine Gogolok, et al.

Updated version	Access the most recent version of this article at: http://clincancerres.aacrjournals.org/content/19/15/4124

Cited Articles	This article cites by 48 articles, 14 of which you can access for free at: http://clincancerres.aacrjournals.org/content/19/15/4124.full.html#ref-list-1

E-mail alerts	Sign up to receive free email-alerts related to this article or journal.
Reprints and Subscriptions	To order reprints of this article or to subscribe to the journal, contact the AACR Publications Department at pubs@aacr.org.
Permissions	To request permission to re-use all or part of this article, contact the AACR Publications Department at permissions@aacr.org.

Anticancer Effects of Niclosamide in Human Glioblastoma

Anja Wieland[1,5], Daniel Trageser[1,5], Sabine Gogolok[1,5], Roman Reinartz[1,5], Heike Höfer[1,5], Mihaela Keller[1,5], Anke Leinhaas[5], Ramona Schelle[1,5], Sabine Normann[1,5], Lil Klaas[1,5], Andreas Waha[2], Philipp Koch[5], Rolf Fimmers[1], Torsten Pietsch[2], Anthony T. Yachnis[6], David W. Pincus[7], Dennis A. Steindler[7], Oliver Brüstle[5], Matthias Simon[3], Martin Glas[1,4], and Björn Scheffler[1,5]

Abstract

Purpose: Glioblastoma is a highly malignant, invariably fatal brain tumor for which effective pharmacotherapy remains an unmet medical need.

Experimental Design: Screening of a compound library of 160 synthetic and natural toxic substances identified the antihelmintic niclosamide as a previously unrecognized candidate for clinical development. Considering the cellular and interindividual heterogeneity of glioblastoma, a portfolio of short-term expanded primary human glioblastoma cells (pGBM; $n = 21$), common glioma lines ($n = 5$), and noncancer human control cells ($n = 3$) was applied as a discovery platform and for preclinical validation. Pharmacodynamic analysis, study of cell-cycle progression, apoptosis, cell migration, proliferation, and on the frequency of multipotent/self-renewing pGBM cells were conducted *in vitro*, and orthotopic xenotransplantation was used to confirm anticancer effects *in vivo*.

Results: Niclosamide led to cytostatic, cytotoxic, and antimigratory effects, strongly reduced the frequencies of multipotent/self-renewing cells *in vitro*, and after exposure significantly diminished the pGBMs' malignant potential *in vivo*. Mechanism of action analysis revealed that niclosamide simultaneously inhibited intracellular WNT/CTNNB1-, NOTCH-, mTOR-, and NF-κB signaling cascades. Furthermore, combinatorial drug testing established that a heterozygous deletion of the *NFKBIA* locus in glioblastoma samples could serve as a genomic biomarker for predicting a synergistic activity of niclosamide with temozolomide, the current standard in glioblastoma therapy.

Conclusions: Together, our data advocate the use of pGBMs for exploration of compound libraries to reveal unexpected leads, for example, niclosamide that might be suited for further development toward personalized clinical application. *Clin Cancer Res; 19(15); 4124–36. ©2013 AACR.*

Introduction

Chemotherapy has developed as an effective line of defense against cancer (1). In the highly malignant brain tumor glioblastoma, the alkylating agent temozolomide has become a standard, in combination with surgical resec-

tion and radiotherapy. There is nevertheless a considerable need to develop alternative treatments, as glioblastoma remains a fatal disease with a median overall survival time of only 15 months (2, 3). For anticancer drug discovery, two major strategies are traditionally used (4). One is the targeted approach where cancer-related molecules and/or signaling cascades must be identified before specific compounds can be designed for distinct interference and inhibition. Alternatively, empirical screening of thousands of compounds can be conducted to identify otherwise unpredictable antineoplastic effects. Both strategies are burdened with high attrition rates during clinical translation (5, 6). This may in part be caused by the use of inept cellular model systems for drug evaluation at early developmental stages (7), for example, inter- and intrapatient tumor heterogeneity is rarely reflected within these systems. In this regard, primary human cancer cells might provide unique opportunities when applied as a discovery platform.

On the basis of this rationale and based on established conditions for the isolation and maintenance of primary human glioblastoma cells (pGBM) known to retain patient- and disease-specific traits *in vitro* (8–10), we pursued an empirical screening approach. Drug discovery and

Authors' Affiliations: [1]Stem Cell Pathologies, Institute of Medical Biometry, Informatics and Epidemiology, Departments of [2]Neuropathology and [3]Neurosurgery, [4]Division of Clinical Neurooncology, Department of Neurology, University of Bonn Medical Center; [5]Institute of Reconstructive Neurobiology, LIFE & BRAIN Center, University of Bonn and Hertie Foundation, Bonn, Germany; Departments of [6]Pathology and [7]Neurosurgery, University of Florida, Gainesville, Florida

Corresponding Author: Björn Scheffler, Stem Cell Pathologies, Institute of Reconstructive Neurobiology, LIFE & BRAIN Center, University of Bonn and Hertie Foundation, Sigmund Freud Str. 25, D-53105 Bonn, Germany. Phone: 49-228-6885-473; Fax: 49-228-6885-443; E-mail: bscheffler@uni-bonn.de

American Association for **Cancer Research**

Translational Relevance

The last few years have shown that chemotherapy, particularly the alkylating standard agent temozolomide, is a safe and effective adjunct treatment for patients with glioblastoma. The disease remains nevertheless fatal, and innovative preclinical efforts are needed to establish a rationale for future clinical developments and studies. As shown here, the use of short-term expanded, patient-specific cancer cells that portray intra- and interpatient heterogeneity might be ideally suited as a discovery platform for empirical screening. Validation of identified compounds on these cells might furthermore reveal unexpected effects and mechanisms with direct implication for clinical translation.

validation was conducted on a portfolio of pGBMs representing multiple facets of the disease. Human nonmalignant neural cell populations (hnNC) and commonly used glioma cell lines served as a control in these studies. The small-molecule niclosamide emerged as glioblastoma-selective, proapoptotic, antiproliferative compound that, after exposure to pGBMs, significantly increased survival times of xenografted mice. A synergistic combinatorial anticancer effect with temozolomide and an associated biomarker furthermore suggested unique perspectives for future drug developments that might augment current glioblastoma therapy standards.

Materials and Methods

For patient data see Supplementary Table S1.

Tissue samples

Tumor tissue was obtained from glioblastoma surgery and hippocampus tissue (case #155) from epilepsy surgery at the Department of Neurosurgery, University of Bonn (Bonn, Germany). Case #GNV019 glioblastoma tissue was obtained from the Department of Neurosurgery, University of Florida (Gainesville, FL). Local Ethics committees at both sites approved the studies—patients or their guardians, provided informed consent. Tissue diagnosis and grading was based on the classification of the World Health Organization (11).

Tissue handling and cell culture

Media, reagents, and analytic compounds are available from Life Technologies or Sigma-Aldrich. "Standard glioblastoma model" cell lines [LN229, T98G, U87(MG), U138, and U373(MG)] were maintained in Dulbecco's modified Eagle medium (DMEM)/F12–based media supplemented with 10% fetal calf serum (Hyclone; standard conditions; _sm). For some studies, defined media (_dm) were applied to glioblastoma model cell lines for 10 days before initiation of experiments. "_dm" resembles media compositions used for the culture of pGBMs and hnNCs/AHNPs, that is, adapted from ref. (8): N2/B27-supplemented Neurobasal with addition of growth factors every other day [EGF, basic fibroblast growth factor (bFGF); 10 ng/mL each). Handling of tissue and derivation of pGBMs (10), hippocampus-derived adult human neural progenitor cells (AHNP; case #155; ref. 12) and case #GNV019 cells (13) were recently described. Data presented here were obtained from short-term expanded pGBMs and AHNPs (passage 5–12; Supplementary Table S2). With exception of the neurosphere assay, all cells were cultured adherently on laminin/poly-L-ornithine–coated plastic. In addition to AHNPs, two long-term self-renewing neural stem cell cultures (lt-NES) were used as nonmalignant neural control. lt-NESs were derived from the human embryonic stem cell line H9.2 (14) and from the human induced pluripotent stem cell line PKa (15, 16).

Compound screening

Killer Plates (MicroSource) compounds were supplied at 1 µmol/L [0.01% dimethyl sulfoxide (DMSO) for control] 24 hours after seeding 2 to 3×10^3 cells per well into 96-well plates. At day 5, cellular viability was determined using the alamarBlue assay (Life Technologies) and an Infinite200 microplate reader (Tecan) at $\lambda_{ex} = 540$ nm and $\lambda_{em} = 590$ nm. Experiments were carried out in triplicates for each sample. For pharmacodynamic analysis, IC_{50} was defined as compound concentration that reduced the cellular viability by 50% compared with control conditions and determined via data analysis in GraphPad Prism 4.0.

Coculture experiments

Lentiviral transduction and selection of pGBMs was conducted using the pLenti6.2/V5-DEST Gateway Vector harboring the coding sequence of GFP as suggested by the manufacturer (Life Technologies). Flow cytometry confirmed stable cellular expression. Alternatively, pGBMs and hnNCs were labeled with CellTracker (carboxyfluorescein diacetate succinimidyl ester [CFSE] green fluorescent dye or -Red CMTPX; Life Technologies) according to the manufacturer's instructions. For initiation of respective cocultures, cells were mixed at 1:1 ratios and maintained for 24 hours before conducting experimental paradigms. For distinctive monitoring of cell growth, a fluorescence-enabled CellaVista System Analyzer (Roche Diagnostics) was used. Fluorescence-activated cell sorting (FACS) data for endpoint analysis were obtained using a FACSCalibur flow cytometer (BD Biosciences).

Proliferation kinetics

Five days posttreatment, 4.7×10^4 vital cells were plated into 3.5-cm plastic dishes, and 4 to 6 days later trypsinized, harvested, counted, and replated at a density of 4.7×10^4. The procedure was repeated four to five times. Cell growth was monitored using the CellaVista System Analyzer for cellular confluency.

Cell migration

A total of 5×10^4 cells were plated into 12-well plates and treated with 125 nmol/L niclosamide every 24 hours for

4 days. At day 3 (cellular density of 70%), a scratch/wound was inflicted with a sterile pipette tip and media was exchanged to remove nonadherent cells. The Plaque Assay application of the CellaVista System Analyzer was used for monitoring (triplicate analysis ± SEM).

Cell cycle

Cells (5×10^4/well) were grown in 12-well plates, and collected after treatment at indicated time points. Cells were resuspended in PBS, fixed with ice-cold methanol, and incubated for 24 hours at 4°C. Pellets were collected by centrifugation and resuspended in PBS, containing 50 μg/mL propidium iodide (PI) and 50 μg/mL RNase. Following incubation for 30 minutes at 37°C, cells were analyzed for DNA content using the FACSCalibur flow cytometer. The sample size for every experiment was 2×10^4 cells.

Apoptosis

A total of 1×10^5 cells were collected at 5 days following compound application, settled by centrifugation, resuspended in 100 μL Annexin V buffer, and incubated with 5 μL Annexin V–fluorescein isothiocyanate (FITC) for 1 hour at room temperature. To distinguish between living and dead cells, labeling with 1.2 μg/mL Hoechst 33258 was used. Annexin V presence was determined in a LSRII cytometer equipped with FACSDiva Software (BD Biosciences). A total of 2×10^4 cells were counted per measurement. The term "avital cells" referred to Annexin V[+]-, Annexin V[+]/H33258[+], and H33258^{+} cells.

Neurosphere assay

The assay was conducted as described previously (10, 13). Neurospheres were quantified at 21 days in culture, triturated to a single-cell suspension, and replated for analysis of secondary and tertiary neurospheres. Multipotency was determined by plating a representative fraction of 3° neurospheres onto laminin/poly-L-ornithine–coated glass coverslips allowing differentiation for 2 to 3 weeks before fixation in 4% paraformaldehyde (PFA).

Immunocytochemistry

Analysis was conducted on PFA-fixed samples according to the standard protocols (13, 17) using antibodies against βIII tubulin (Promega; monoclonal mouse; 1:1,000), glial fibrillary acidic protein (DAKO; polyclonal rabbit; 1:600), β-catenin, and phospho-β-catenin (Ser552) antibodies (both from Cell Signaling Technology; 1:400). Cell nuclei were visualized with 4′,6-diamidino-2-phenylindole (DAPI; Sigma).

Western blotting

Cell extracts were prepared at 24 to 144 hours following compound application and processed as described previously (18). Blot membranes were incubated overnight at 4°C with antibodies against cyclin D1 (1:1,000; BD Pharmingen), Notch1 (1:1,000), cleaved-Notch1 (1:1,000), S6 ribosomal protein (1:1,000), phospho-S6 protein (1:1,000), or phospho-RELA (p65; Ser536; 1:1,000; all from Cell Signaling Technology), respectively. After washing, peroxidase-coupled secondary antibodies (Santa Cruz Biotechnology) were added for 1 hour. After washing, blots were developed using the enhanced chemiluminescence (ECL) system (Millipore). To confirm equal loading, blots were reprobed with an β-actin antibody (Sigma; 1:5,000).

Quantitative reverse transcription PCR

Total RNA was isolated (RNeasy Mini Kit; Qiagen), quantified (Nanodrop; Peqlab), and 400 ng was reversely transcribed with oligo-dT primers in a reaction mix ($1\times$ RT-Puffer, 10 mmol/L dithiothreitol [DTT], 500 μmol/L pooled dNTPs, 1 U/μL RNase inhibitor, and 2.5 U/μL Expand Reverse Transcriptase; Roche Diagnostics). Reaction occurred at 42°C for 1 hour. The cDNA product was amplified in a total volume of 10 μL in 96-well plates using the realplex 4 Mastercylcer Ep Gradient S (Eppendorf) at: 95°C for 2 minutes, followed by 40 cycles of 95°C for 15 seconds, 60°C for 20 seconds, and 72°C for 30 seconds. The following primers were used: S100A4 forward, 5′-CTCAGCG-CTTCTTCTTTC-3′; S100A4 reverse, 5′–GGGTCAGCAGC-TCCTTTA-3′; c-Myc forward, 5′–TTCGGGTAGTGGAA-AA-CCAG-3′; c-Myc reverse, 5′-CAGCAGCTCGAATTTCTTCC-3′; cyclin D1 forward, 5′–CCGTCCATGCGGAAGATC-3′; cyclin D1 reverse, 5′–ATGGCCAGCGGGAAGAC-3′; NFK-BIA forward, 5′–ACACCAGGTCAGGATTTTGC-3′; NFKBIA reverse, 5′-GCTGATGTCAATGCTCAGGA-3); GAPDH forward, 5′-TGCACCACCAACTGCT-TAGC-3; GAPDH reverse, 5′–GGCATGGACTGTGGTCATGAG-3′. Data were analyzed with the Mastercycler Ep Realplex Software (Eppendorf). Mean values were calculated from triplicate reactions. Each mean value of expressed genes was normalized to the mean amount of the respective housekeeping glyceraldehyde-3-phosphate dehydrogenase (GAPDH) cDNA.

Single-nucleotide polymorphism array analysis

Evaluation of the *NFKBIA* locus was conducted on the basis of genotyping data of the respective samples [pGBMs; 299,140 single-nucleotide polymorphism (SNP); Illumina HUMANCytoSNP-12 v2.1; Infinium HD assay; Illumina], or based on public data (glioblastoma cell lines; http://www.ncbi.nlm.nih.gov/geo/query/acc.cgi?acc = GSE13021). Analysis with Illumina GenomeStudio (2011.1) software included the Genotyping and GenomeViewer modules. Chromosomal aberrations were identified by examination of log R ratios and B-allele frequencies.

MGMT promoter status

Methylation of the *MGMT* gene was determined by pyrosequencing as described recently (19).

Orthotopic xenografts

The Ethical Committee of the University of Bonn approved all animal studies. $Rag2^{-/-}Il2rg^{-/-}$ mice were acquired from Taconic Farm Inc., contractor of the National Institute of Allergy and Infectious Diseases' investigators (20). SCID/Beige mice were purchased from The Jackson Laboratory. For transplantation, cells were harvested,

counted, and resuspended in 0.1% DNase/PBS. Cell vitality was confirmed via Trypan blue exclusion. For case #046, 10^6 DMSO-control ($n = 5$)- or niclosamide ($n = 5$)–pretreated pGBMs were unilaterally injected into the striatum of 12-week-old Rag2Il2rg$^{-/-}$ mice (0.8 mm anterior, 2 mm lateral, 3 mm deep). Similarly, engrafted naïve case #046 cells were additionally used for in vivo analysis of niclosamide. Treatment was initiated at day 62 posttransplantation and consisted of intraperitoneal application of 30 mg/kg niclosamide in solvent, or solvent solution (control; 10% Cremophor EL; 0.9% NaCl; according to ref. 21) for 3×5 days. For case #GNV019, 2.5×10^4 sham control (Killer Plates compound 2F05; $n = 9$)- or niclosamide ($n = 6$)–pretreated pGBMs were injected intracranially into P2 to P3 old SCID/Beige mice. Mice were monitored daily and euthanized when signs of distress/neurologic symptoms or significant weight loss was noted. The case #GNV019 experiment was terminated at day 169 with one remaining animal that did not seem distressed. For subsequent histologic analysis, brains were removed, cryoprotected, and serially cut on a cryostat (Leica) at 20 μm thickness. Every fifth section underwent standard hematoxylin and eosin (H&E) staining for histologic analysis of tumor formation.

Statistical analysis

GraphPad Prism 4.0 software was used. Data with error bars represent triplicate experiments (mean ± SD) unless otherwise noted. P values for Figs. 3C and E and 6C and F were determined using two-way ANOVA. For multiple comparisons, P values were calculated using the one-way ANOVA with Bonferroni post hoc test. If applicable, the two-sided Student t test was used to determine statistical significance ($P < 0.05$).

Results

Niclosamide is a previously unrecognized candidate for glioblastoma therapy

The Killer Plates compound library comprising 160 synthetic and natural toxic substances was used for empirical screening. In many ways, this collection represents other commercial or experimental libraries containing known drugs next to less characterized (e.g., natural) substances that are potentially able to induce otherwise unpredictable (e.g., antineoplastic) effects. The major goal of our study was to test whether heterogeneous pGBMs were suited to identify previously unconsidered new drug candidates—and/or mechanisms that could be applied to current therapeutic settings. Four pGBMs, previously shown to maintain patient- and glioblastoma-specific signatures and to contain subpopulations of tumor cells with and without multipotent/self-renewing qualities, were used as a discovery platform (cases #023, #035, #046, and #106; ref. 10). The screening was conducted using the alamarBlue assay to determine the metabolic activity as a measure of cellular viability 5 days after single application of the library's compounds (1 μmol/L; Supplementary Table S3). Every compound that reduced the mean metabolic activity of the

four pGBMs to less than 50% control levels was considered as a "hit." Thirty-one compounds fulfilled this criterion (Fig. 1A), but only 25 indicated a sufficient potential to address interpatient heterogeneity, impacting effectively on all four of the tested pGBMs (Fig. 1B and E). Among these, 10 "hits" showed a cancer-specific potential, as they did not similarly affect hnNC case #155, a control case of nonmalignant primary AHNPs (ref. 12; Fig. 1C and E). Noteworthy, a variety of strategies could be used to prioritize "hit compounds" for follow-up experiments. Here, we opted for an array of five criteria (see Fig. 1E). The first three were intended to identify compounds that (criterion #1) effectively inhibited the cellular viability of (criterion #2) a diversity of pGBMs, without (criterion #3) similarly affecting human neural control cells. The remaining two criteria focused on novelty: many existing compound libraries have already been empirically screened using "standard glioblastoma models," for example, as part of the NCI60 collection. We were thus curious to select in this study for compounds that may have been overlooked in the past. pGBM "hit compounds" that did not show activity in the standard U87 model system were therefore considered as a positive selection example (criterion #4; Fig. 1D). Similarly, compounds already under clinical investigation were excluded (case #5). From this array of criteria, only niclosamide emerged (Fig. 1E). Niclosamide is an established antihelminthic drug for which recent work in extra-neural, for example, preclinical colorectal cancer models had already suggested antineoplastic activity (21, 22). This encouraged further assessment as a candidate compound for glioblastoma therapy.

Niclosamide effectively and selectively inhibits glioblastoma cell viability

To validate the screening results, pharmacodynamic analysis was conducted using a formulation of niclosamide from an independent supplier (Sigma-Aldrich). A total of 21 pGBMs were investigated. The obtained dose–response curves showed consistent courses for all of these samples (Fig. 2A). The respective IC$_{50}$ values ranged from 300 nmol/L to 1.2 μmol/L. This contrasted to the more resistant attributes of reference- and control-samples. Of note, 2.4- to 4.2-fold higher IC$_{50}$ values were found in the commonly investigated glioma/glioblastoma cell lines LN229, T98G, U87, U138, and U373 that were used here as a reference (Fig. 2B and Supplementary Fig. S1).

It has frequently been suggested (e.g., ref. 7) that "standard glioblastoma models," maintained in standard serum media (_sm) may have lost specific traits during the decade-long period of their use in the field. Consequently, we investigated whether defined media conditions (_dm) used for the culture of pGBMs and hnNCs would alter the sensitivity of these cell lines to niclosamide. Data from pharmacodynamic analysis confirmed this assumption, showing pGBM-like degrees of sensitivity to niclosamide (Fig. 2B, bottom inset; Supplementary Fig. S2). Thus, niclosamide appeared as candidate agent that would not have been identified if "standard glioblastoma models/conditions" were used for empirical screening.

Considering the cellular and genetic diversity that characterizes glioblastoma, we next investigated niclosamide's pharmacologic effect in an array of pGBMs reflecting key clinical constellations (10, 23–25). Comparative experiments were carried out with samples derived from (i) the tumor core (center) versus periphery region of the same patient with glioblastoma, (ii) primary versus recurrent disease of the same patient with glioblastoma, (iii) *MGMT*-promoter hypermethylated versus unmethylated tissue, and from (iv) glioblastomas with heterozygous-deleted *NFKBIA* versus -undeleted *NFKBIA* genotypes. In all of the respective pGBMs, similar pharmacodynamic results were obtained (top inset Fig. 2B; Supplementary Fig. S1), portraying niclosamide as a highly effective inhibitor of the different molecular subtypes of pGBMs.

Notably, analysis of the three nonmalignant hnNCs that were maintained in defined and mitogen-supplied culture conditions similar to pGBMs revealed a significantly lower level of sensitivity (Fig. 2B and Supplementary Fig. S1). To confirm the putative glioblastoma-selective activity of niclosamide, we conducted coculture experiments combining hnNC case #155 with various pGBMs. Continuous monitoring and endpoint FACS analysis after exposure to the compound indeed revealed that niclosamide selectively inhibited pGBMs (Fig. 2C and D).

Cytostatic, cytotoxic, and antimigratory effects of niclosamide in pGBMs

To classify the inhibitory activity of niclosamide, cell cycle, vitality, and migratory activity were investigated
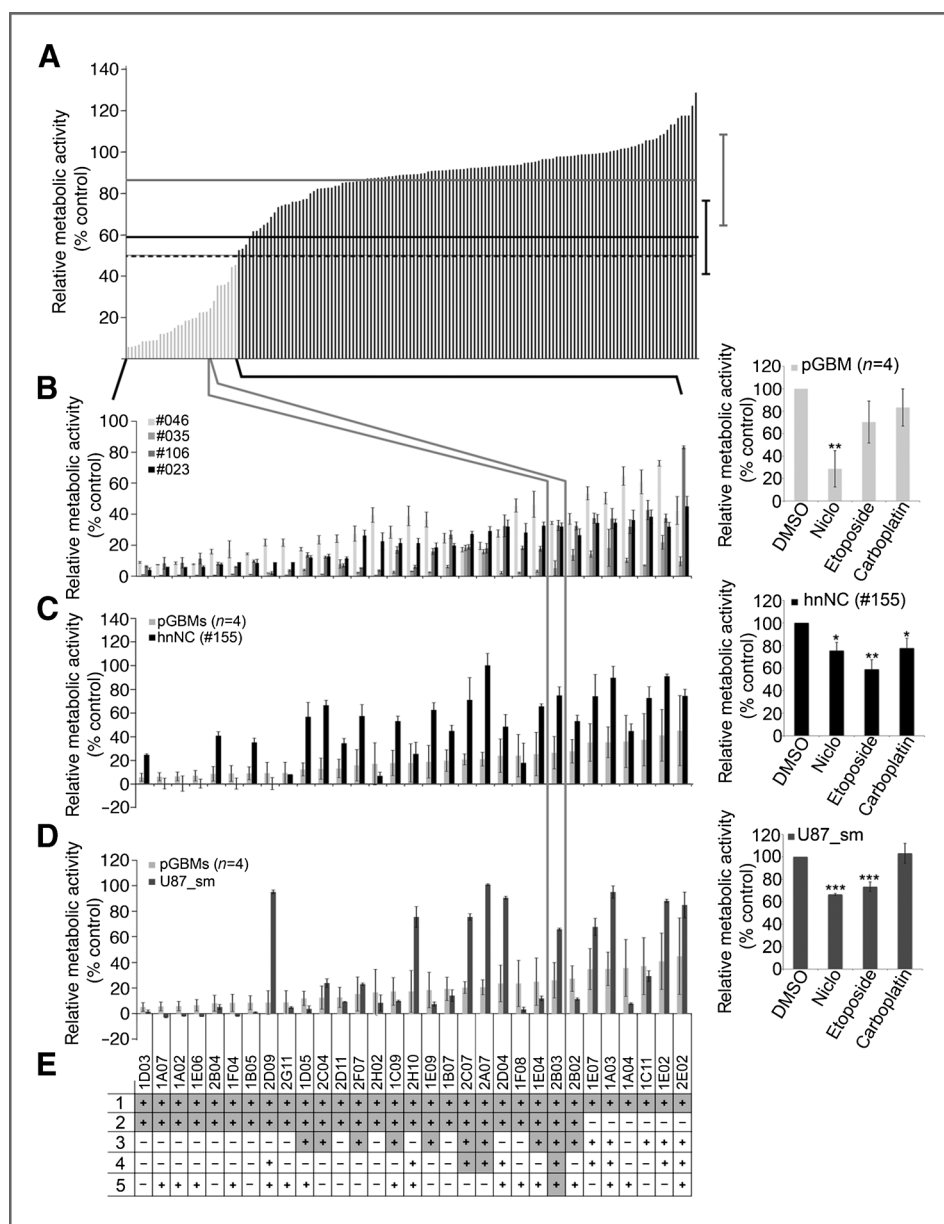

Figure 1. Primary screening of the Killer Plates identifies niclosamide (Niclo) as lead compound. A, pGBMs (cases #023, #035, #046, and #106) were exposed to the library's 160 compounds (1 µmol/L) for 5 days. The graph arranges mean data relative to controls. Respective temozolomide responses are indicated for reference including error bars (right; 50 µmol/L, gray line; 500 µmol/L, black line). Thirty-one "hits" were identified [light gray bars; 50% level indicated as dotted line; individual "hit" data in (B), triplicate analysis; mean ± SD]. hnNCs (C; case #155) and the U87 glioma cell line (D; maintained in standard media; _sm) were investigated in parallel. Insets in (B)–(D) compare niclosamide data to respectively investigated control compounds. E, selection criteria for niclosamide (2B03) as a lead compound: 1 = mean relative metabolic activity <50%; 2 = relative metabolic activity <50% in all four pGBMs; 3 = relative metabolic activity >50% in hnNCs; 4 = relative metabolic activity >50% in U87_sm; 5 = compound not in clinical use or in clinical studies on patients with glioma. Compounds coded according to Killer Plate-identifiers (Supplementary Table S3; ***, $P < 0.001$; **, $P < 0.01$; *, $P < 0.05$).
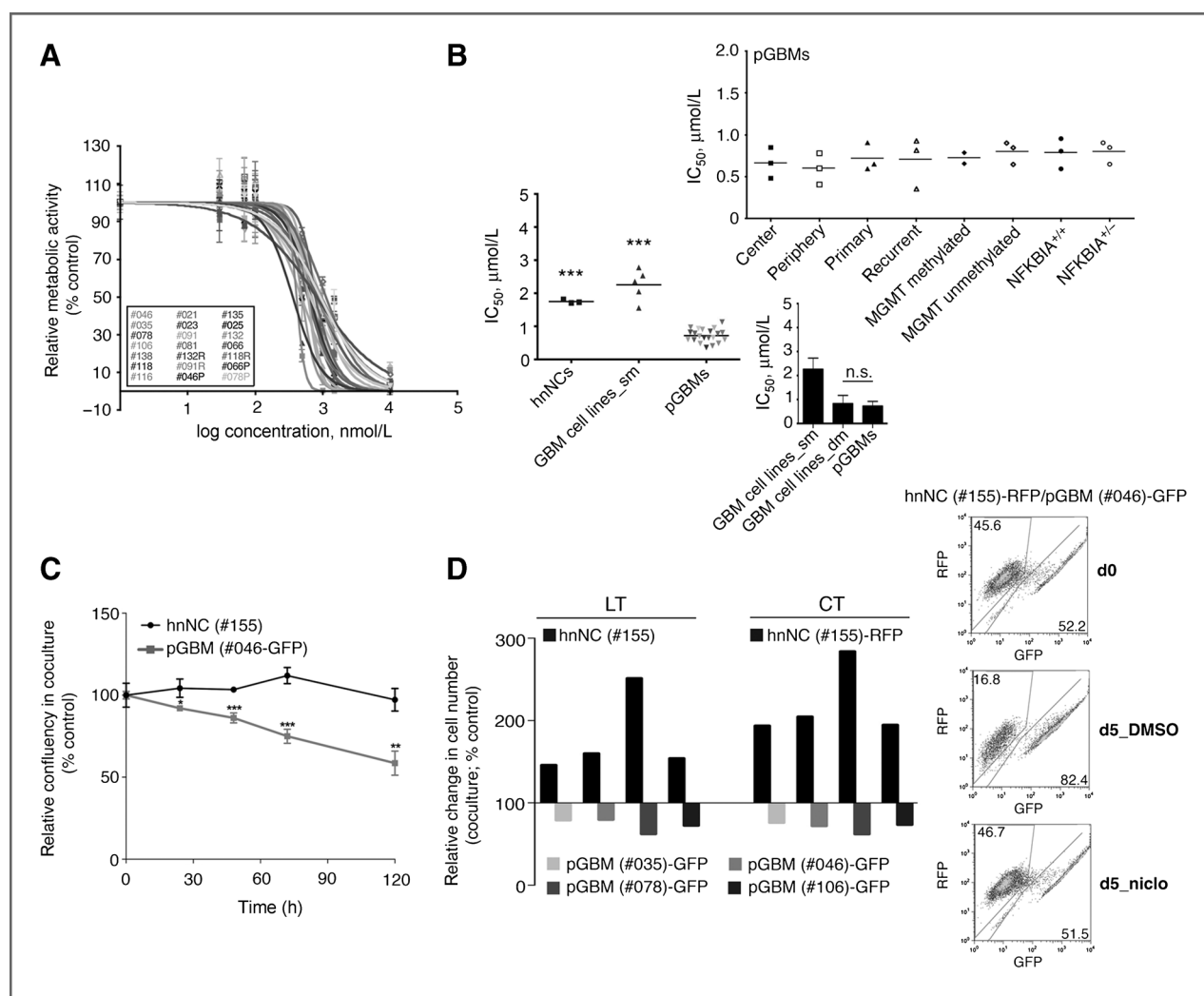
Figure 2. Niclosamide (niclo) effectively and selectively inhibits glioblastoma cell viability. A, pharmacodynamic analysis of 21 pGBMs (cases indicated) at day 5 following exposure to niclosamide (concentration indicated). Data as mean $\pm$ SD of triplicates. B, spectrum of IC_{50} values representing the concentrations that decrease the metabolic activity to 50% of control levels. Data collected from three hnNCs (see Materials and Methods), five commercially available glioma/glioblastoma cell lines (standard media, _sm; see Materials and Methods), and 21 pGBMs [see (A) and Supplementary Table S1]. The top inset depicts IC_{50} data from additional pair-wise comparative experiments (symbol coded) on pGBMs derived from tumor center versus periphery, from primary versus recurrent disease, from *MGMT* promoter hypermethylated versus unmethylated specimens, and from samples with *NFKBIA*^{+/+} versus heterozygous *NFKBIA*-deleted genotypes (*NFKBIA*^{+/−}). The lower inset additionally depicts IC_{50} data obtained from niclosamide-treated glioblastoma cell lines maintained in defined media (_dm; $n = 5$; mean $\pm$ SD). P values (***, $P < 0.001$) were calculated from comparing hnNCs and glioblastoma cell line data with pGBMs, respectively, using the one-way ANOVA and Tukey *post hoc* tests. n.s., not significant. C, CellaVista-based analysis of cocultures. Data were obtained at indicated time points after application of niclosamide (1 µmol/L). Triplicate analysis (***, $P < 0.001$; **, $P < 0.01$). D, FACS data obtained 5 days after application of niclosamide (1 µmol/L) to respective cocultures. The inset depicts a representative set of scatter plots. Note that pGBMs cases #046 and #078 are NFKBIA^{+/−}; cases #035 and #106 are NFKBIA^{+/+} genotypes. LT, lentivirally transduced; CT, CellTracker-labeled populations.

after a single exposure of the compound. Flow cytometry analysis showed a transient G_1 arrest of pGBMs peaking at 24 to 48 hours (Fig. 3A and Supplementary Fig. S3). This coincided with a strong decrease of CCND1 (cyclin D1) expression, a regulator of the transition from G_1 to S phase (Fig. 3B). Consequently, examination of pGBM's growth kinetics revealed a transient cytostatic effect (Fig. 3C). At 5 days following compound exposure, an additional cytotoxic response was noted by phase contrast microscopy (not shown) and quantified by flow cytometry (Fig. 3D). Intriguingly, subtoxic concentrations of

niclosamide also caused antimigratory effects on pGBMs, similar to recent findings described for colon cancer cells (ref. 21; Fig. 3E).

Niclosamide inhibits the malignant potential of pGBMs

We next aimed to investigate the influence of niclosamide on the malignant potential of the heterogeneous cell populations present in pGBMs. An experimental paradigm was designed to study cells that survived a single dose niclosamide (20%–30% remain vital at this concentration, compare Fig. 3D). *In vitro* monitoring of pGBMs ($n = 4$) showed that
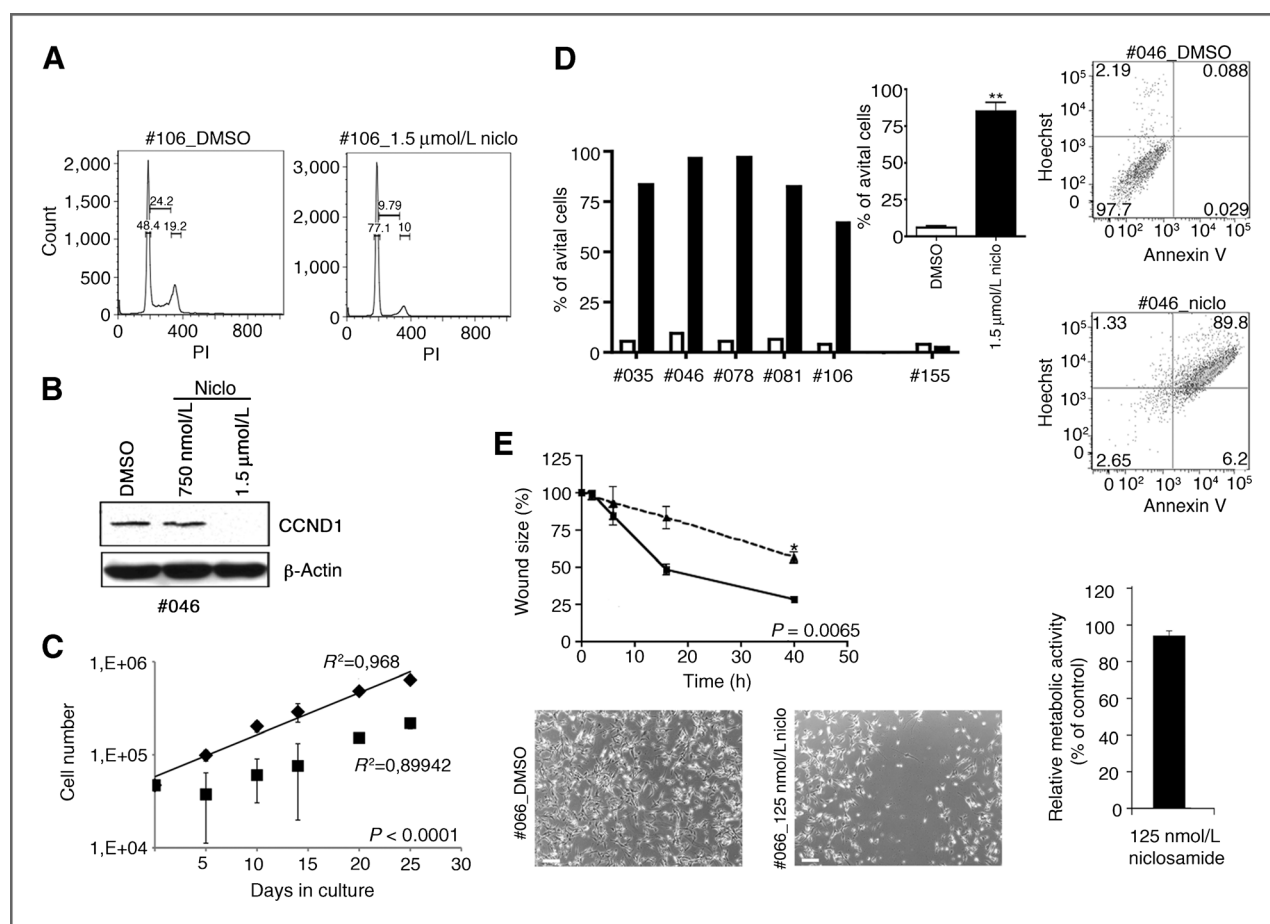
Figure 3. Cytostatic and cytotoxic effects of niclosamide. A, cell-cycle analysis at 24 hours after application (2×10^4 cells each). Note the increased G_1 peak in the niclosamide (niclo)-treated sample. B, cyclin D1 (CCND1)-Western blot analysis derived at this time point. Full-length blot in Supplementary Fig. S4A. C, growth kinetics after single niclosamide exposure (1.5 µmol/L; squares) or DMSO (0.01%; rhombi; pGBM cases #046, #078, and #106; mean $\pm$ SD). D, frequency of avital, that is, Annexin V^+ and/or Hoechst 33258^+ cells 5 days after application of niclosamide (black bars) or 0.01% DMSO (white bars). Inset, mean data. Note the lack of proapoptotic effects in hnNC case #155. Right, representative scatter plots (case #046). E, scratch assay ($n = 2$ pGBMs; mean $\pm$ SD; triplicate analysis). Time course shown for case #046 (125 nmol/L niclosamide, dotted line; 0.0025% DMSO, solid line); phase contrasts for case #066 at 24 hours. Inset, right, cellular viability at day 5 following compound application. Scale bars, 50 µmol/L. (**, $P < 0.01$; *, $P < 0.05$).

these cells regained proliferative activity after compound application (Fig. 4A and C). Xenografting of naïve versus preexposed vital pGBM cells was then performed to determine whether these populations conducted similarly *in vivo*. We hypothesized that the survival time of engrafted animals would remain unchanged if niclosamide preexposure would not influence the malignant potential of pGBMs. Yet, in comparison with naïve cell grafts, animals receiving similar numbers of preexposed vital pGBMs survived significantly longer (Fig. 4B and D). This extension could not solely be explained by a potential growth disadvantage of vital preexposed cells. From the *in vitro* monitoring studies, a delay of 14 to 23 days would have been expected (compare Fig. 4A and C). However, pGBM case #GNV019 engrafted animals that died from naïve cell tumor growth after 44 ± 6 days did not show evidence for tumor formation for up to 233 days when engrafted with preexposed cells (Fig. 4B). pGBM case #046 cells that formed large tumors after 88 ± 5 days showed smaller, developing tumors at 153 ± 23 days after engraft-

ment, when preexposed to niclosamide (Fig. 4D). Histologic analysis consistently revealed massive intracerebral tumors after unilateral intrastriatal application of naïve case #046 cells and a strong invasive potential of individual engrafted cells along white matter tracts toward the contralateral hemisphere (Fig. 4E). In contrast, tumors that developed in 4 of 5 animals from niclosamide preexposed case #046 pGBMs were smaller in size with cells accumulating in areas adjacent to the transplant site (Fig. 4F). Mitotic active pGBMs clustered in the subventricular zone and dispersed from there through the corpus callosum (inset Fig. 4F). Apparently, this diffuse invasion sufficed in the long-term *in vivo* experiments to induce distress in the animals that required euthanization even before an expanding tumor mass manifested. In a preliminary study, we additionally investigated systemic administrations of niclosamide to xenografted animals in which intracerebral tumors had already been established (Fig. 4G). This experiment, however, showed only a trend toward extended survival ($P = 0.0549$), which at least in part
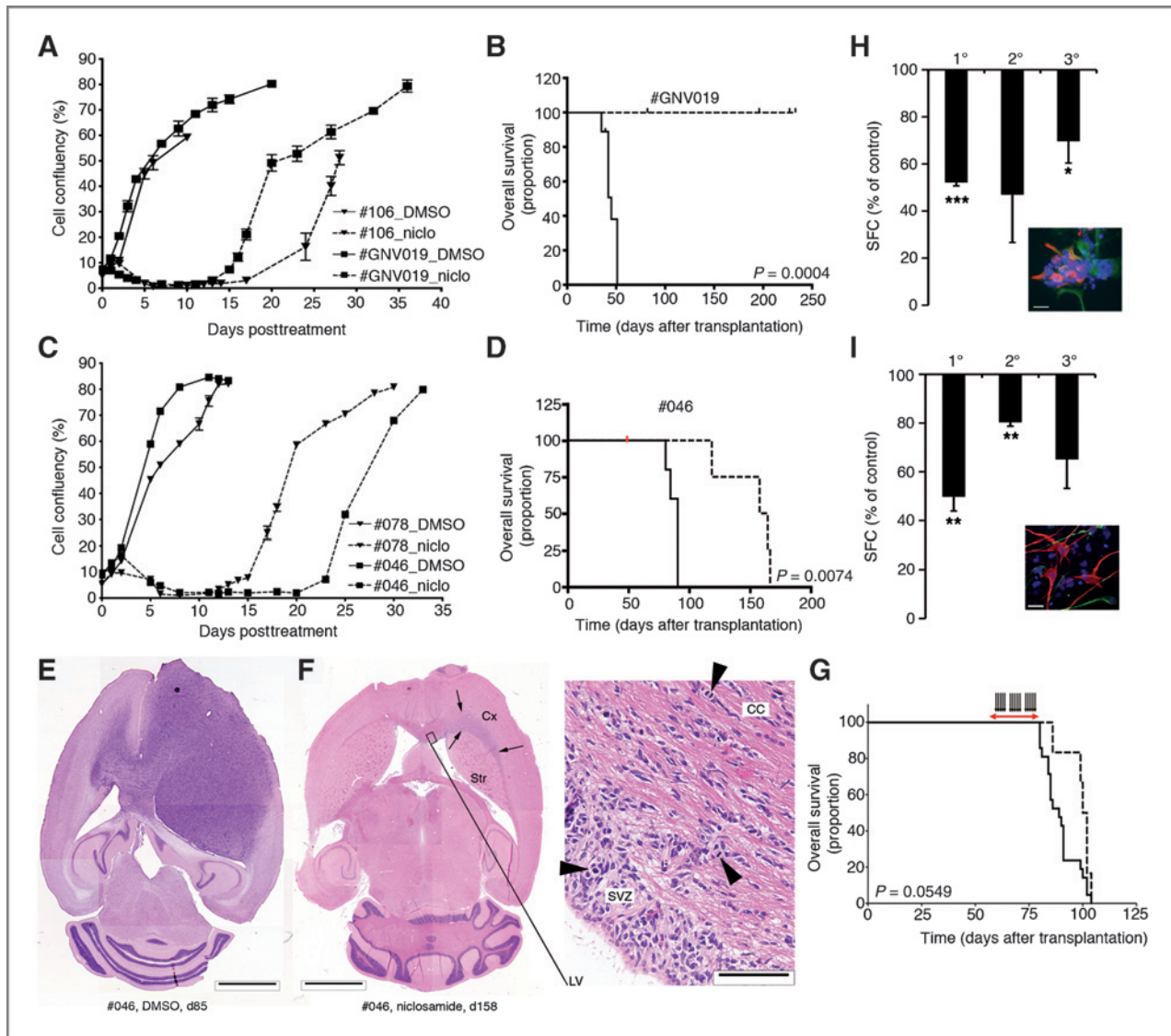
Figure 4. Niclosamide (niclo) inhibits the malignant potential of pGBMs. Data from *NFKBIA*$^{+/+}$- (A, B, and H) and *NFKBIA*$^{+/-}$- (C-G, and I) pGBM genotypes. A, long-term cell growth data after single niclosamide application (niclo; dotted lines) versus 0.01% DMSO (solid lines; mean ± SD; triplicates). B, Kaplan–Meier survival curves depicting DMSO-pretreated (solid; tumor manifestation in 8 of 9 animals) versus niclosamide (dotted) preexposed cell xenografts. Note, no animal receiving niclosamide preexposed grafts showed evidence for tumor formation (censored events). C, *in vitro* data (similar to A). D, Kaplan–Meier survival curves (similar to B). Intracerebral tumors manifested in all but one animal (niclosamide; red dot). E, DMSO-typic, H&E-stained horizontal brain section exposing a right hemispheric tumor mass and diffusely crossing/invading tumor cells (collage, 85 days after engraftment). F, niclosamide-typic, H&E-stained horizontal brain section (collage, 158 days following engraftment) showing only few tumor cells at the site of initial engraftment, distributing between cortical (Cx) and striatal (Str) aspects (arrows). The inset exposes mitotically active (arrowheads) glial tumor cells in the subventricular zone (SVZ) of (F) diffusely invading the adjacent corpus callosum (CC). LV, lateral ventricle. Scale (E) and (F), 2 mm; (F) inset, 100 μmol/L. G, *in vivo* pilot study (pGBM case #046; see Materials and Methods). Naïve tumor cell accumulation was validated at day 50 and 60 after transplantation (*n* = 2 animals each). Niclosamide treatment [30 mg/kg body weight intraperitoneally (i.p.); according to ref. 21)] was initiated at day 62 (15×/3 weeks; indicated by arrows). All animals showed intracerebral tumors (solvent-treated, solid; niclosamide-treated, dotted). Calculation of *P* values (B, D, and G) based on the log-rank test. H, neurosphere assay (*n* = 2 pGBMs in triplicate; mean ± SD). The graph depicts the relative frequency of primary (1°), secondary (2°), and tertiary (3°) neurospheres from niclosamide preexposed pGBMs (single exposure). Note the persistent decrease of sphere-forming cells (SFC). The inset visualizes neuronal (βIII tubulin; red) and glial (GFAP; green) differentiation potential of remaining cells from 3° neurospheres (case #GNV019 shown). Scale bar, 25 μm. I, neurosphere data (similar to G). The inset visualizes neuronal (βIII tubulin; green) and glial (GFAP; red) differentiation potential of remaining cells from 3° neurospheres (case #046 shown; scale bar, 50 μm). ***, *P* < 0.001; **, *P* < 0.01; *, *P* < 0.05. GFAP, glial fibrillary acidic protein.

could be due to the "pilot" character of our investigation, for example, the limited number of animals studied and the used experimental setting, including the choice of timing and dosage of compound applications.

Our preexposure experiments nevertheless suggested that niclosamide has an inhibitory impact on the malignant potential of pGBM cells. One potential explanation for the extended survival of animals engrafted with

preexposed cells is an effect on the self-renewing/multipotent cell fraction that in the past had been related to tumor initiation (e.g., refs. 26–29). In previous studies, we had established their frequencies in the range from 0.25% to 1% among our culture passage 5 to 10 pGBMs (10). Here, the neurosphere assay was used to estimate potential niclosamide-induced alterations to this pool of cells. Quantification of 1° to 3° spheres from DMSO- versus niclosamide preexposed cells indeed indicated that a single application of the compound reduced the frequencies of self-renewing/multipotent pGBM cells considerably ($n = 4$; Fig. 4H and I).

Niclosamide interferes with cancer-driving signaling cascades

A circumscribed number of transcription factors and signaling pathways are overly active in human cancer cells (30). Evidence from previous studies had suggested that niclosamide interfered with several of these in non-neural cancer cells, specifically affecting the NOTCH-, mTOR-, WNT-/CTNNB1-, and NF-κB signaling cascades (21, 22, 31–33). We focused on these cascades for mechanism of action analysis. pGBMs were investigated at day 5 after a single-dose exposure ($n = 4$; cases #046, #078, #081, and #106). Western blot analyses showed a concentration-
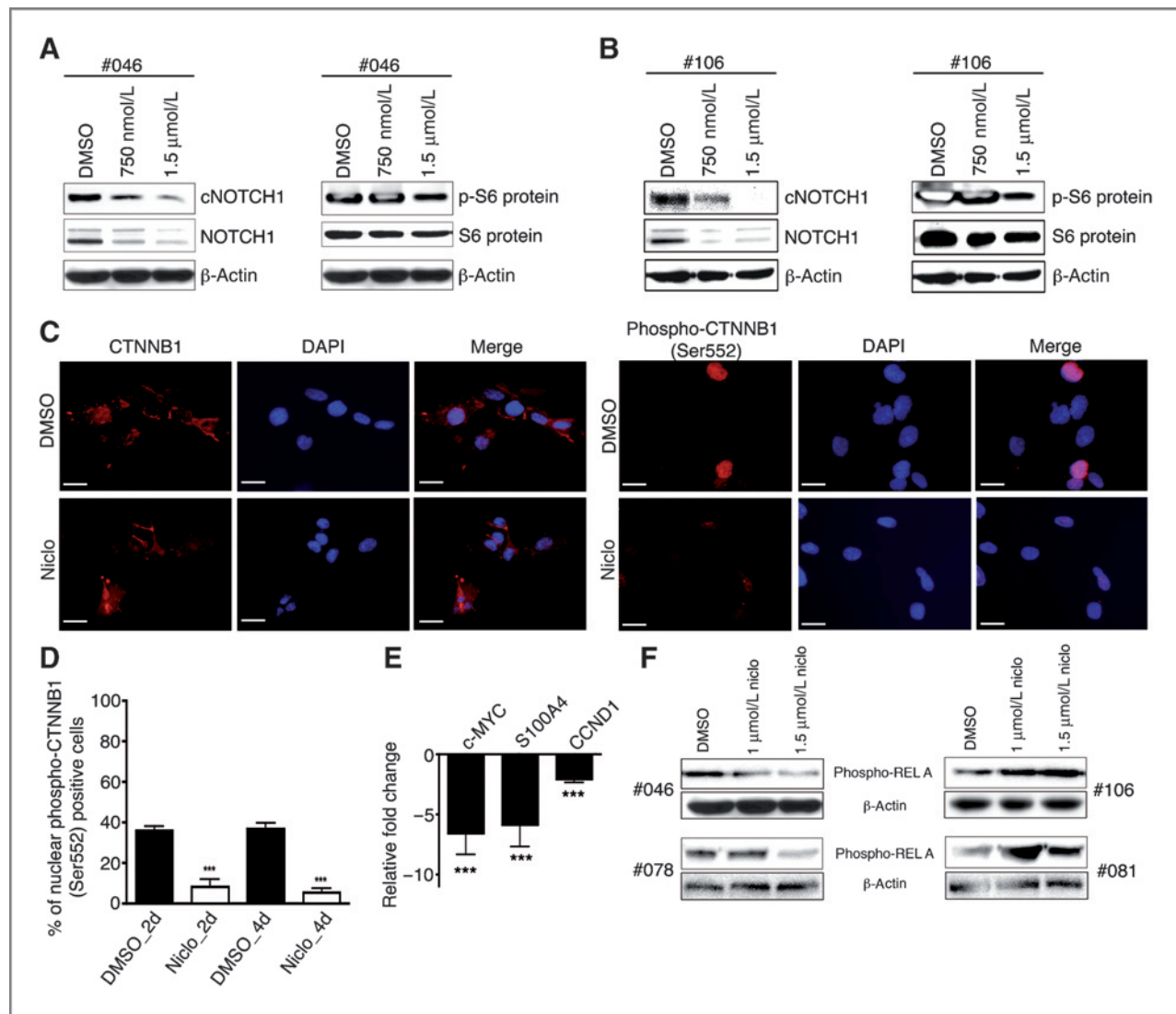

Figure 5. Pleiotropic anticancer effects of niclosamide (Niclo). Representative Western blot analyses from (A) NFKBIA$^{+/-}$- and (B) NFKBIA$^{+/+}$-genotypes obtained at day 5 after single-dose application ($n = 4$ pGBMs analyzed). C, immunofluorescence analysis of CTNNB1 (β-catenin) and phospho-CTNNB1 (Ser552) in pGBMs ($n = 3$; case #0106 shown) 2 days after application of 1.5 μmol/L niclosamide (blue, DAPI; scale bars 20 μm). D, quantification of nuclear phospho-CTNNB1 (Ser552)$^+$ cells ($n = 3$; ***, $P < 0.001$; triplicates; mean ± SD). E, quantitative reverse transcription PCR (qRT-PCR) of WNT/CTNNB1 target genes ($n = 3$; ***, $P < 0.001$; triplicates; mean ± SD). Expression relative to DMSO control. P values calculated using one-way ANOVA analysis with Bonferroni post hoc test. F, representative Western blot analyses of phospho-RELA (p65-NF-κB) in (left) NFKBIA$^{+/-}$- and (right) NFKBIA$^{+/+}$-genotypes at day 3 after single-dose application ($n = 6$ pGBMs analyzed). Full-length blots are presented in Supplementary Fig. S4.
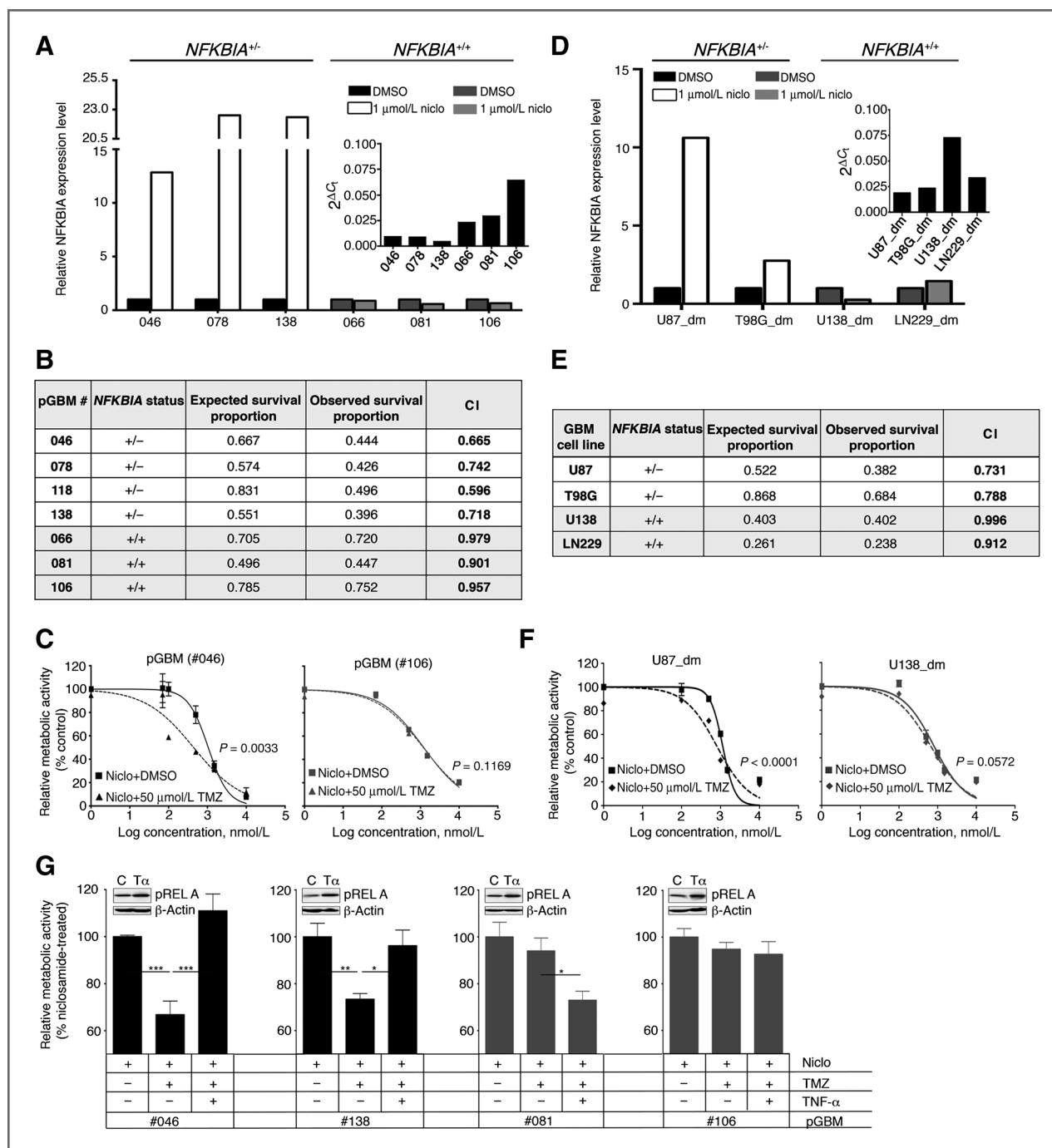
Figure 6. Deletion and expression level of *NFKBIA* predicts synergistic activity of niclosamide (Niclo) and temozolomide (TMZ). A–C, and G, data from analysis of pGBMs; D–F, data from analysis of standard glioblastoma (GBM) cell lines maintained in defined media conditions (_dm). A, changing mRNA levels in *NFKBIA*$^{+/+}$ (gray) versus *NFKBIA*$^{+/-}$ (black/white) pGBMs in response to niclosamide (relative to DMSO control). Inset, baseline mRNA expression levels of NFKBIA. B, CI evaluation for application of niclosamide + temozolomide in pGBMs. CIs were expressed as ratio of observed versus expected cell viability. Expected results were calculated according to ref. (42) as proportion of viable cells after treatment with (only) 1 μmol/L niclosamide multiplied by the proportion of cells following treatment with (only) temozolomide. (CI < 1: synergy; CI = 1: additive; CI>1:antagonism). C, representative combinatorial pharmocodynamics of temozolomide and niclosamide in *NFKBIA*$^{+/-}$ (left) versus *NFKBIA*$^{+/+}$ (right) pGBMs. Increasing concentrations of niclosamide were supplied either in combination with 50 μmol/L temozolomide or with 0.05% DMSO as control. Data presented as mean ± SD of triplicates. D, quantification of mRNA levels, similar to (A). E, evaluation of CI values, similar to (B). F, combinatorial pharmocodynamics, similar to (C). G, TNF-α antagonizes synergistic activity in *NFKBIA*$^{+/-}$ pGBMs. Graphs present data from combinatorial treatment schedules in *NFKBIA*$^{+/-}$ (black) versus *NFKBIA*$^{+/+}$ (gray) pGBMs at 3 days after compound application (niclo, 1 μmol/L; temozolomide, 50 μmol/L; TNF-α 50 ng/mL). Insets, Western blot analyses of pREL A, indicating NF-κB pathway activity 24 hours after exposure to TNF-α (Tα; 50 ng/mL) or 0.002% bovine serum albumin (C; control). ***, $P < 0.001$; **, $P < 0.01$; *, $P < 0.05$. (triplicates; mean ± SD; one-way ANOVA and Tukey *post hoc* tests). CI, combinatorial index.

dependent inhibition of NOTCH pathway activity and expression, indicated by decreasing levels of NOTCH1 and cleaved NOTCH1-protein (Fig. 5A and B). Similarly, decreasing levels of the phosphorylated S6-protein were observed as an indication for repression of active mTOR signaling (ref. 34; Fig. 5A and B). Exploration of the WNT/CTNNB1 pathway suggested that niclosamide furthermore interfered with the noncanonical (alternative) AKT-dependent regulation of CTNNB1's transcriptional activity. Characteristic for the active state of this mechanism, known to play an important role for tumor invasion, is an enhanced nuclear accumulation of CTNNB1, phosphorylated at Ser[552] (35). Immunocytochemical detection (Fig. 5C) and quantification (Fig. 5D) of this antigen showed its strongly decreased presence in the nuclei of pGBMs in response to niclosamide. Consequently, the expression of CTNNB1 target genes decreased significantly (Fig. 5E; refs. 21, 36, 37). Thus, niclosamide revealed a pleiotropic mechanism of action in pGBMs, inhibiting major cancer-driving signaling cascades simultaneously.

In contrast to the consistent inhibition of these pathways, niclosamide exhibited a variable effect on NF-κB signaling, as evidenced by analysis of phospho-REL A (p65-NF-κB) protein expression (Fig. 5F). Pathway inhibition could only be revealed in pGBMs (cases #046 and #078) that showed a distinctive heterozygous deletion of the NFKBIA locus (NFKBIA^{+/−}) at 14q13. This finding intrigued, because recent work had suggested that deletion and low expression of NFKBIA, encoding for a repressor of intracellular NF-κB signaling, is associated with unfavorable clinical outcomes and temozolomide chemotherapy resistance in patients with glioblastoma (25).

NFKBIA predicts synergistic effects of niclosamide and temozolomide

We next aimed to understand the differential effect of niclosamide on the NF-κB signaling pathway in relation to the NFKBIA genotype. Baseline expression levels of NFKBIA coincided with the respective genomic status in pGBMs from our cohort ($n = 3$ each group) as well as in "standard glioblastoma models" ($n = 2$/group; _dm conditions; inset Fig. 6A and D). Upon exposure to niclosamide, NFKBIA^{+/−} pGBMs and glioblastoma cell lines strongly upregulated their initially low expression levels, while NFKBIA^{+/+} samples did not (Fig. 6A and D). As upregulation of NFKBIA expression goes along with inhibition of NF-κB activity, this finding might explain why niclosamide inhibits the activity of this pathway in NFKBIA^{+/−}, but not in NFKBIA^{+/+} samples (compare Fig. 5F). Interestingly, NF-κB inhibitors are known to sensitize to anticancer drugs, and downregulation of NFKBIA in glioblastoma cells and tissue is associated with a lack of response to O^6-alkylating agents, for example, the standard glioblastoma chemotherapeutic temozolomide (38). Bredel and colleagues (25) have recently shown that retrovirally mediated reexpression of NFKBIA in NFKBIA-deleted glioblastoma cell models can lead to reversal of temozolomide resistance. Because our data suggested niclosamide as a "natural inducer" of

NFKBIA expression in NFKBIA^{+/−} samples, we next investigated for a potential benefit of combined niclosamide/temozolomide application in our samples.

Seven pGBMs and four standard glioblastoma cell lines (_dm conditions) with known NFKBIA status (Fig. 6B, C, E, and F) underwent combinatorial drug testing. Noteworthy, all the pGBM samples showed an unmethylated MGMT promoter status, a condition that indicates poor clinical responses to temozolomide-based glioblastoma chemotherapy (Supplementary Table S1; ref. 2, 25). Combinatorial index (CI) analysis of niclosamide was conducted in the presence of 50 μmol/L temozolomide. The concentration of temozolomide was based on the reported plasma peak level (39), which is known to impact very little on the viability of glioma cells in vitro (10, 40, 41). Similarly, we here observed that 50 μmol/L temozolomide reduced the viability of pGBMs and glioblastoma cell lines to only 94% ± 4% and 89% ± 8% of control levels, respectively ($n = 7 + 4$; data not shown). In combination with niclosamide, however, a strong synergistic effect was noted selectively in NFKBIA^{+/−}-pGBMs and -glioblastoma cell lines (Fig. 6B and E). Their dose–response curves left-shifted compared with NFKBIA^{+/+} samples (Fig. 6C and F). CI calculation (42) of niclosamide/temozolomide revealed nearly additive effects in NFKBIA^{+/+}-pGBMs (CI, 0.94 ± 0.04), and strong synergistic effects in NFKBIA^{+/+}-samples (CI, 0.68 ± 0.06; Fig. 6B). Similar genotype-dependent data were obtained from glioblastoma cell lines (Fig. 6E). To directly show the involvement of NF-κB in the observed synergistic activity, we conducted control studies using the NF-κB activator TNF-α (Peprotech). Application of TNF-α activated NF-κB in pGBMs, and in accordance to our hypothesis, counteracted synergy effects in NFKBIA^{+/−} genotypes (Fig. 6G).

Together, our data suggest that niclosamide can augment anticancer effects of the standard therapeutic temozolomide and that the genomic status of NFKBIA could predict a synergistic effect of the combined drugs in glioblastoma.

Discussion

Significant therapies for patients with glioblastoma are limited. In search for new therapeutic options, our study set out at the earliest time point of anticancer drug development. The results of our work have a variety of implications. First, we could show that short-term expanded patient-specific cells can be useful tools for the identification of previously unconsidered new drug candidates. An advantage of appropriate collections of these cells is that inter- and intrapatient heterogeneity becomes accessible for compound screening. Moreover, we provide a reason for future reinvestigation of known compound libraries, as previous screening approaches on "standard glioblastoma models" (under standard conditions) could have overlooked promising lead compounds.

Secondly, the identification of niclosamide's anticancer effects might provide promising cues for future developments in the field of personalized glioblastoma therapy. Its overall efficient inhibitory effects combined with a lack of differential activity against the different molecular subtypes

of glioblastoma cells can be considered a strength of niclosamide. This feature could be ideally suited to counteract inter- and intrapatient heterogeneity characteristically observed in this type of cancer (43)—at concentrations that affect human nonmalignant neural (control) cells only slightly. This broad effect could be a result of niclosamide's pleiotropic activity, similarly affecting signaling pathways that are known to be overly active in human malignant cells (i.e., mTOR, NOTCH, WNT/CTNNB1; refs. 44–46). Our preexposure paradigm furthermore suggested a thorough effect on the malignant potential of pGBMs *in vivo*. However, challenges for immediate clinical translation of our findings are, for example, the hitherto unknown optimum application route and the defining of appropriate dosage schedules for the compound. Niclosamide is approved as antihelminthic by many regulatory agencies, but it has not yet been considered for brain tumor therapy. It is a salicylanilide that was introduced as a molluscide in 1959. Studies in animals suggested no mutagenic, oncogenic, or embryotoxic activity and no cumulative effects; however, its rate of absorption from the intestinal tract was estimated at only 33% (for review see ref. 47). Our pilot experiment on established xenograft-derived intracerebral tumors could only preliminarily address this issue. For example, for choice of application route and dosage, we have relied on previously reported methods used in an animal model on the metastatic progression in colon cancer (21). Future experiments are required to address these open questions.

A third aspect of our work relates to the potential mechanism of synergy between temozolomide and niclosamide as a "natural inducer" of NFKBIA. The resulting inhibition of NF-κB activity could be used to overcome resistance to temozolomide (38), at least in $NFKBIA^{+/-}$ glioblastoma genotypes. It would moreover be reasonable to assume that other cancer entities presenting with specific SNPs and haplotypes of the $NFKBIA$ locus, for example, Hodgkin's lymphoma, colorectal cancer, melanoma, hepatocellular carcinoma, breast cancer, and multiple myeloma (see ref. 25) might profit from combinatorial therapeutic regimens in the settings of personalized medicine. Even though the status of the $NFKBIA$ locus as a predictor for synergy needs further validation—both, in preclinical and in clinical settings, our data provide a rationale for future targeted screening attempts to identify alternative combinatorial compounds that take advantage of this mechanism.

In perspective, data from our study encourage the use of short-term expanded, patient-specific cancer cells as a discovery platform for new or previously neglected lead compounds. Appropriate portfolios of primary cells might portray intra- and interpatient heterogeneity to an unanticipated degree, perhaps adding benefit to current efforts on the establishment of alternative predictive models for anticancer drug sensitivity (48).

Authors' Contributions
Conception and design: A. Wieland, M. Simon, M. Glas, B. Scheffler
Development of methodology: A. Wieland, S. Gogolok, D.A. Steindler, M. Glas, B. Scheffler
Acquisition of data (provided animals, acquired and managed patients, provided facilities, etc.): A. Wieland, D. Trageser, S. Gogolok, R. Reinartz, H. Höfer, M. Keller, A. Leinhaas, R. Schelle, S. Normann, P. Koch, T. Pietsch, D.W. Pincus, D.A. Steindler, M. Simon, B. Scheffler
Analysis and interpretation of data (e.g., statistical analysis, biostatistics, computational analysis): A. Wieland, A. Waha, R. Fimmers, A.T. Yachnis, D.A. Steindler, O. Brüstle, M. Glas, B. Scheffler
Writing, review, and/or revision of the manuscript: A. Wieland, D. Trageser, R. Reinartz, T. Pietsch, D.A. Steindler, M. Simon, M. Glas, B. Scheffler
Administrative, technical, or material support (i.e., reporting or organizing data, constructing databases): L. Klaas, T. Pietsch, O. Brüstle
Study supervision: M. Glas, B. Scheffler
Other: P. Koch, provision of material; R. Schelle, unspecified contribution.

References
1. Chabner BA, Roberts TG Jr. Timeline: chemotherapy and the war on cancer. Nat Rev Cancer 2005;5:65–72.
2. Hegi ME, Diserens AC, Gorlia T, Hamou MF, de Tribolet N, Weller M, et al. MGMT gene silencing and benefit from temozolomide in glioblastoma. N Engl J Med 2005;352:997–1003.
3. Stupp R, Hegi ME, Mason WP, van den Bent MJ, Taphoorn MJ, Janzer RC, et al. Effects of radiotherapy with concomitant and adjuvant temozolomide versus radiotherapy alone on survival in glioblastoma in a randomised phase III study: 5-year analysis of the EORTC-NCIC trial. Lancet Oncol 2009;10:459–66.
4. Swinney DC, Anthony J. How were new medicines discovered? Nat Rev Drug Discov 2011;10:507–19.
5. Kola I, Landis J. Can the pharmaceutical industry reduce attrition rates? Nat Rev Drug Discov 2004;3:711–5.
6. Damia G, D'Incalci M. Contemporary pre-clinical development of anticancer agents—what are the optimal preclinical models? Eur J Cancer 2009;45:2768–81.
7. Sharma SV, Haber DA, Settleman J. Cell line-based platforms to evaluate the therapeutic efficacy of candidate anticancer agents. Nat Rev Cancer 2010;10:241–53.
8. Lee J, Kotliarova S, Kotliarov Y, Li A, Su Q, Donin NM, et al. Tumor stem cells derived from glioblastomas cultured in bFGF and EGF more closely mirror the phenotype and genotype of primary tumors than do serum-cultured cell lines. Cancer Cell 2006;9:391–403.
9. Pollard SM, Yoshikawa K, Clarke ID, Danovi D, Stricker S, Russell R, et al. Glioma stem cell lines expanded in adherent culture have tumor-specific phenotypes and are suitable for chemical and genetic screens. Cell Stem Cell 2009;4:568–80.

10. Glas M, Rath BH, Simon M, Reinartz R, Schramme A, Trageser D, et al. Residual tumor cells are unique cellular targets in glioblastoma. Ann Neurol 2010;68:264–9.

11. Louis DN, Ohgaki H, Wiestler OD, Cavenee WK, Burger PC, Jouvet A, et al. The 2007 WHO classification of tumours of the central nervous system. Acta Neuropathol 2007;114:97–109.

12. Walton NM, Sutter BM, Chen HX, Chang LJ, Roper SN, Scheffler B, et al. Derivation and large-scale expansion of multipotent astroglial neural progenitors from adult human brain. Development 2006;133: 3671–81.

13. Scheffler B, Walton NM, Lin DD, Goetz AK, Enikolopov G, Roper SN, et al. Phenotypic and functional characterization of adult brain neuropoiesis. Proc Natl Acad Sci U S A 2005;102:9353–8.

14. Koch P, Opitz T, Steinbeck JA, Ladewig J, Brustle O. A rosette-type, self-renewing human ES cell-derived neural stem cell with potential for in vitro instruction and synaptic integration. Proc Natl Acad Sci U S A 2009;106:3225–30.

15. Falk A, Koch P, Kesavan J, Takashima Y, Ladewig J, Alexander M, et al. Capture of neuroepithelial-like stem cells from pluripotent stem cells provides a versatile system for in vitro production of human neurons. PLoS ONE 2012;7:e29597.

16. Koch P, Breuer P, Peitz M, Jungverdorben J, Kesavan J, Poppe D, et al. Excitation-induced ataxin-3 aggregation in neurons from patients with Machado-Joseph disease. Nature 2011;480:543–6.

17. Goetz AK, Scheffler B, Chen HX, Wang S, Suslov O, Xiang H, et al. Temporally restricted substrate interactions direct fate and specification of neural precursors derived from embryonic stem cells. Proc Natl Acad Sci U S A 2006;103:11063–8.

18. Wiechen K, Diatchenko L, Agoulnik A, Scharff KM, Schober H, Arlt K, et al. Caveolin-1 is down-regulated in human ovarian carcinoma and acts as a candidate tumor suppressor gene. Am J Pathol 2001;159: 1635–43.

19. Mikeska T, Bock C, El-Maarri O, Hubner A, Ehrentraut D, Schramm J, et al. Optimization of quantitative MGMT promoter methylation analysis using pyrosequencing and combined bisulfite restriction analysis. J Mol Diagn 2007;9:368–81.

20. Cao X, Shores EW, Hu-Li J, Anver MR, Kelsall BL, Russell SM, et al. Defective lymphoid development in mice lacking expression of the common cytokine receptor gamma chain. Immunity 1995;2:223–38.

21. Sack U, Walther W, Scudiero D, Selby M, Kobelt D, Lemm M, et al. Novel effect of antihelminthic Niclosamide on S100A4-mediated metastatic progression in colon cancer. J Natl Cancer Inst 2011;103: 1018–36.

22. Osada T, Chen M, Yang XY, Spasojevic I, Vandeusen JB, Hsu D, et al. Antihelminth compound niclosamide downregulates Wnt signaling and elicits antitumor responses in tumors with activating APC mutations. Cancer Res 2011;71:4172–82.

23. Simpson L, Galanis E. Recurrent glioblastoma multiforme: advances in treatment and promising drug candidates. Expert Rev Anticancer Ther 2006;6:1593–607.

24. Weller M, Stupp R, Reifenberger G, Brandes AA, van den Bent MJ, Wick W, et al. MGMT promoter methylation in malignant gliomas: ready for personalized medicine? Nat Rev Neurol 2010;6:39–51.

25. Bredel M, Scholtens DM, Yadav AK, Alvarez AA, Renfrow JJ, Chandler JP, et al. NFKBIA deletion in glioblastomas. N Engl J Med 2011;364: 627–37.

26. Stiles CD, Rowitch DH. Glioma stem cells: a midterm exam. Neuron 2008;58:832–46.

27. Zhou BB, Zhang H, Damelin M, Geles KG, Grindley JC, Dirks PB. Tumour-initiating cells: challenges and opportunities for anticancer drug discovery. Nat Rev Drug Discov 2009;8:806–23.

28. Nguyen LV, Vanner R, Dirks P, Eaves CJ. Cancer stem cells: an evolving concept. Nat Rev Cancer 2012;12:133–43.

29. Westphal M, Lamszus K. The neurobiology of gliomas: from cell biology to the development of therapeutic approaches. Nat Rev Neurosci 2011;12:495–508.

30. Darnell JE Jr. Transcription factors as targets for cancer therapy. Nat Rev Cancer 2002;2:740–9.

31. Balgi AD, Fonseca BD, Donohue E, Tsang TC, Lajoie P, Proud CG, et al. Screen for chemical modulators of autophagy reveals novel therapeutic inhibitors of mTORC1 signaling. PLoS ONE 2009;4: e7124.

32. Wang AM, Ku HH, Liang YC, Chen YC, Hwu YM, Yeh TS. The autonomous notch signal pathway is activated by baicalin and baicalein but is suppressed by niclosamide in K562 cells. J Cell Biochem 2009;106:682–92.

33. Jin Y, Lu Z, Ding K, Li J, Du X, Chen C, et al. Antineoplastic mechanisms of niclosamide in acute myelogenous leukemia stem cells: inactivation of the NF-kappaB pathway and generation of reactive oxygen species. Cancer Res 2010;70:2516–27.

34. Wullschleger S, Loewith R, Hall MN. TOR signaling in growth and metabolism. Cell 2006;124:471–84.

35. Fang D, Hawke D, Zheng Y, Xia Y, Meisenhelder J, Nika H, et al. Phosphorylation of beta-catenin by AKT promotes beta-catenin transcriptional activity. J Biol Chem 2007;282:11221–9.

36. Clevers H. Wnt/beta-catenin signaling in development and disease. Cell 2006;127:469–80.

37. Moon RT, Kohn AD, De Ferrari GV, Kaykas A. WNT and beta-catenin signalling: diseases and therapies. Nat Rev Genet 2004;5: 691–701.

38. Bredel M, Bredel C, Juric D, Duran GE, Yu RX, Harsh GR, et al. Tumor necrosis factor-alpha-induced protein 3 as a putative regulator of nuclear factor-kappaB-mediated resistance to O^6-alkylating agents in human glioblastomas. J Clin Oncol 2006;24:274–87.

39. Brada M, Judson I, Beale P, Moore S, Reidenberg P, Statkevich P, et al. Phase I dose-escalation and pharmacokinetic study of temozolomide (SCH 52365) for refractory or relapsing malignancies. Br J Cancer 1999;81:1022–30.

40. Hermisson M, Klumpp A, Wick W, Wischhusen J, Nagel G, Roos W, et al. O^6-methylguanine DNA methyltransferase and p53 status predict temozolomide sensitivity in human malignant glioma cells. J Neurochem 2006;96:766–76.

41. Beier D, Rohrl S, Pillai DR, Schwarz S, Kunz-Schughart LA, Leukel P, et al. Temozolomide preferentially depletes cancer stem cells in glioblastoma. Cancer Res 2008;68:5706–15.

42. Chou TC. Drug combination studies and their synergy quantification using the Chou-Talalay method. Cancer Res 2010;70:440–6.

43. Bonavia R, Inda MM, Cavenee WK, Furnari FB. Heterogeneity maintenance in glioblastoma: a social network. Cancer Res 2011;71: 4055–60.

44. Zhang N, Wei P, Gong A, Chiu WT, Lee HT, Colman H, et al. FoxM1 promotes beta-catenin nuclear localization and controls Wnt target-gene expression and glioma tumorigenesis. Cancer Cell 2011;20: 427–42.

45. Zhu TS, Costello MA, Talsma CE, Flack CG, Crowley JG, Hamm LL, et al. Endothelial cells create a stem cell niche in glioblastoma by providing NOTCH ligands that nurture self-renewal of cancer stem-like cells. Cancer Res 2011;71:6061–72.

46. Akhavan D, Cloughesy TF, Mischel PS. mTOR signaling in glioblastoma: lessons learned from bench to bedside. Neuro Oncol 2010;12: 882–9.

47. Andrews P, Thyssen J, Lorke D. The biology and toxicology of molluscicides, Bayluscide. Pharmacol Ther 1982;19:245–95.

48. Barretina J, Caponigro G, Stransky N, Venkatesan K, Margolin AA, Kim S, et al. The cancer cell line encyclopedia enables predictive modelling of anticancer drug sensitivity. Nature 2012;483:603–7.